Application Note

Optomechanical mass sensing

Zurich Instruments

Applications: Sensors, Photonics
Products: MFLI, HF2LI, UHFLI

Release date: January 2022

Introduction

Conventional mass spectrometers classify analytes by measuring their mass-to-charge ratio and can resolve single atoms [1, 2]. However, their low dynamic range limits weighing heavier analytes such as colloidal and aerosol particles larger than only a few atoms. Dissociation methods are often used to fragment such particles, changing their native properties and making the reconstruction of the mass spectrum a challenging work. By contrast, optomechanical sensors measure mass by monitoring the optical modulation transduced by the dynamics of a mechanical system such as a micro-resonator. They offer novel mass sensing schemes with a wider dynamic range and pico- to attogram sensitivity. Further, they enable in situ analysis thanks to their non-destructive nature.

An optomechanical sensor's design can take many forms depending on the environment it operates in and the nature of the particles it probes. To illustrate possible applications, we look at three scenarios:

- Optical balance for single aerosol particles isolated under atmospheric conditions [3].
- Nanomechanical mass spectrometry (NMS) for deposited nanoparticles [4].
- Transparent microcapillary resonators (TMRs) for colloids [5, 6].

In each case, a Zurich Instruments lock-in amplifier provides the signal to drive the mechanical system and extracts the resulting optical modulation separating it from the background.

Optical balance for aerosols

Studies on a single aerosol particle monitor their behavior under atmospheric conditions and provide insights on cloud physics and chemistry by accurate particle characterization. Submicron–sized aerosol particles are particularly important thanks to their contribution to sunlight scattering and absorption [7]. In this size range, the optical balance enables in-situ particle mass measurements down to a few picograms without the need for preconditioning the particle by precharging or depositing it on a substrate [3].

This approach works by isolating a single aerosol particle suspended in an environmental chamber using a counter-propagating optical tweezer as illustrated in Figure 1. With this design it is possible to manipulate the particle position along the beam axis z by altering the power balance between the two counter-propagating laser beams. An optical modulator is responsible for varying the power balance by rotating the laser beam's polarization before a polarizing beam splitter. Modulating the polarization at a frequency f results in a periodic particle motion monitored by a position-sensitive photodetector. The Zurich Instruments MFLI, a digital 5-MHz lock-in amplifier, completes this scheme by providing the periodic drive signal to the optical modulator and by demodulating the photodetector signal to capture the phase delay φ in the particle's motion.

A periodically moving particle in the environmental chamber under atmospheric pressure experiences a drag force. In the case of aqueous droplets, the particle is spherical with radius r. Therefore, the drag force arising from its motion is given by Stokes' law, which

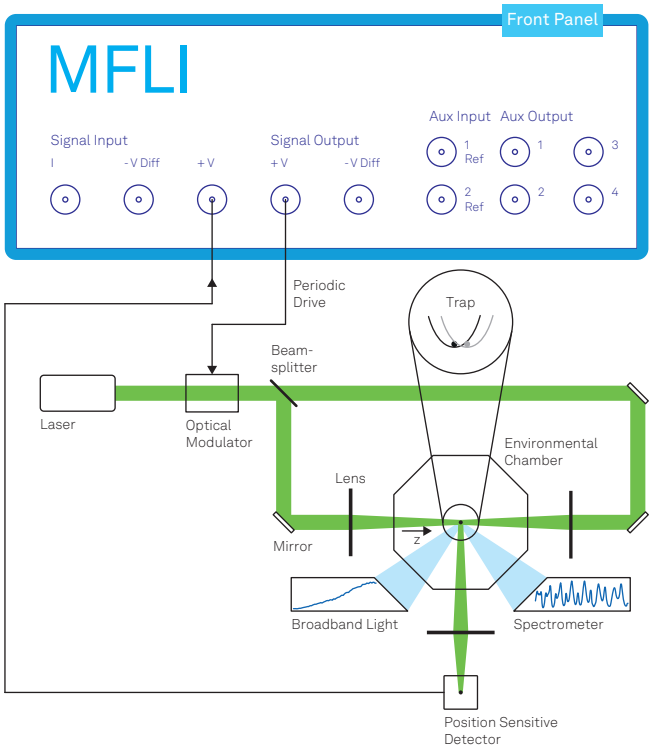

Figure 1. The optical balance scheme. A counter-propagating optical tweezer that traps a single particle and modulates its position along the z axis. The MFLI Lock-in Amplifier drives this modulation by controlling the optical modulator and detects the resulting phase delay in the particle's motion by demodulating the signal from the position-sensitive detector. As the measurement results indicate, the trapping potential can be approximated as a harmonic potential that its center is modulated as depicted in the inset. The optical scheme in this figure is reproduced from [3] under CC BY license.

defines the damping rate Γ as

$$\Gamma = 3r\mu/mC_c, \tag{1}$$

where μ is the dynamic viscosity of the surrounding fluid, nitrogen in this case, and C_c is Cunningham's correction factor [8]. Based on this equation, determining the particle's mass is possible by measuring the damping rate and the particle's size. The latter is measured using a broadband light scattering spectrometer [9]. It illuminates the particle with broadband light in the wavelength range between 300 nm and 500 nm. The intensity profile of the elastically scattered broadband light depends on the particle's size, shape and refractive index [10]. Typical intensity profiles of the incident and scattered broadband light are shown in Figure 1.

The damping rate is determined based on the measured phase delay in the particle's motion. Assuming this is a purely harmonic motion in the form of $z(t) = \sin(2\pi ft - \varphi)$, it is possible to model it as a driven damped harmonic oscillator:

$$\frac{d^2z}{dt^2} + 2\pi\Gamma\frac{dz}{dt} + 4\pi^2 f_r{}^2 z = 4\pi^2 f_r^2 Z\sin(2\pi ft), \tag{2}$$

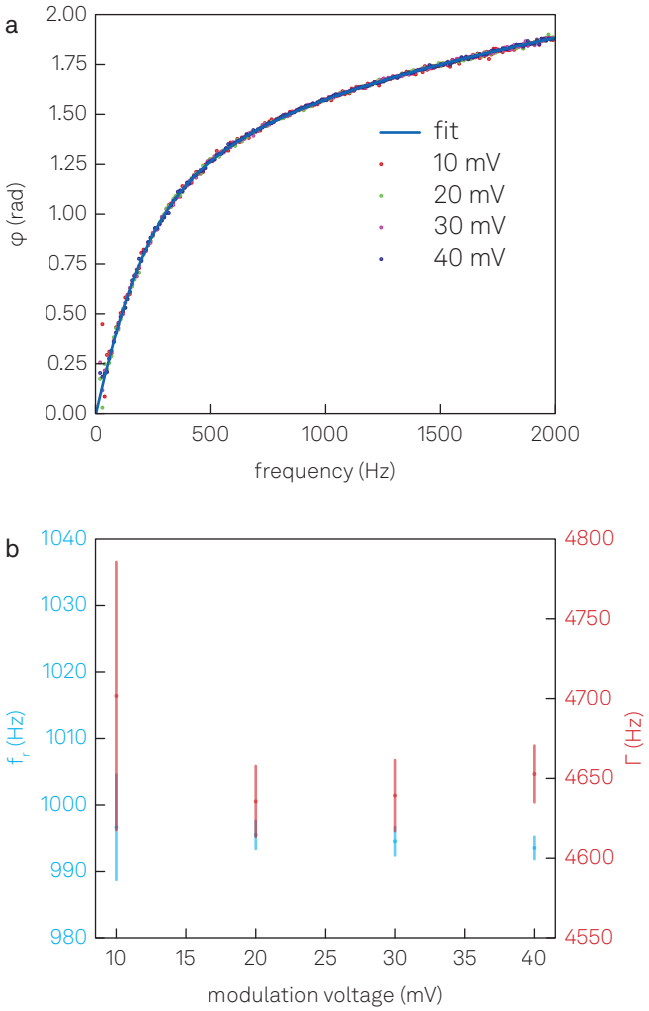

Figure 2. Characterization of the optical balance. (a) Frequency dependence of the phase delay at various modulation amplitudes. (b) The resonance frequency and damping rate determined by fitting the frequency-dependent phase delay with Equation 3. The plots in this figure are adapted from [3] under CC BY license by changing the color scheme and fonts.

where f_r is the natural frequency. The right-hand side of this equation is the modulation term with amplitude Z. The resulting frequency-dependent phase delay becomes a function of the damping rate given by

$$\varphi = \operatorname{atan}\left(\frac{\Gamma f}{f_r^2 - f^2}\right). \tag{3}$$

Fitting this term to the measured phase delay leads to the damping rate.

Reich and collaborators demonstrate the performance of this technique with aqueous-NaCl droplets, which equilibrate with the surrounding humidity rapidly [3]. This makes it possible to test the optical balance with varying particle sizes and densities. To determine Γ and f_r based on Equation 3, they sweep the frequency of the excitation tone generated by one of the built-in oscillators of the MFLI Lock-in Amplifier using the parametric Sweeper, a tool for measurement automation provided by LabOne®, the

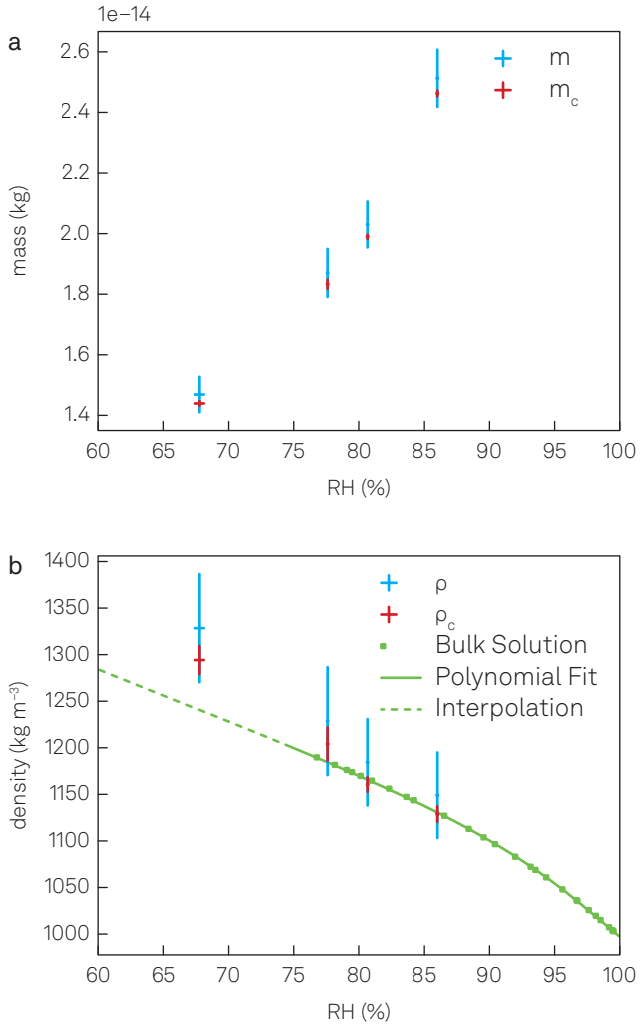

Figure 3. Measurement results with the optical balance. (a) The mass m of a single aqueous-NaCl droplet at varying relative humidities measured using an optical balance. (b) The particle density ρ is calculated from the mass and size r of the particle. The panel also includes the bulk solution density in the subsaturation regime [11]. The plots in this figure are adapted from [3] under CC BY license by changing the color scheme and fonts.

instrument control software of Zurich Instruments. The Sweeper tool captures the phase delay and amplitude corresponding to the swept frequencies while automatically adjusting the demodulator settings of the lock-in amplifier to ensure an optimal signal-to-noise ratio at each frequency step. Figure 2 (a) shows the results from repeated measurements that have no clear dependence on the modulation amplitude. Equation 3 fits well in all cases, and provides the values of Γ and f_r that are given in Figure 2 (b). This independence with respect to the modulation amplitude indicates that the particle is experiencing a harmonic motion and that higher-order terms are negligible.

Once the damping rate Γ and the particle's size r are known, plugging them into Equation 1 provides the particle's mass. Figure 3 shows the results for a single particle at varying relative humidities. Above 75.3±0.3% relative humidity, the aqueous-NaCl solution is undersaturated [11]. In this regime, the particle density agrees well with bulk solution measurements from the literature. However, aerosol particles can supersaturate while remaining in the liquid phase. This measurement clearly shows that extrapolating bulk solution measurements to the saturated regime does not provide the correct results.

The accuracy of the optical balance lies in the range of 6%. This value is influenced by systematic measurement errors and the statistical spread of the measurements. Further improvements on the accuracy are possible by correcting systematic measurement errors with the undersaturated bulk solution densities. This results in an improved 2.5% accuracy that corresponds to $\backsim$100 fg as depicted by m_c in panel (a) and ρ_c in panel (b) of Figure 3 [3].

Nanomechanical mass spectrometry

Nanomechanical mass spectrometry (NMS) measures the mass of deposited particles on a nanoelectromechanical resonator. The natural frequency of the resonator is related to its effective mass. Therefore, a frequency shift occurs when a particle lands on the resonator surface. Monitoring such frequency shifts yields the added mass after an initial characterization of the resonator's natural frequency. This approach is well-suited to the measurement of nanparticle masses thanks to its high sensitivity down to 10^{-21} g and its broad dynamic range [12, 13, 14]. Further, it can monitor the sequential adhesion of many particles on the resonator, hence enabling ensemble measurements.

Figure 4 illustrates the experimental setup developed by Malvar and co-workers [4], which uses a single clamped beam as a cantilever. The beam is attached to an actuator and placed inside a vacuum chamber. The Zurich Instruments HF2LI Lock-in Amplifier provides the drive signal to the actuator to excite the cantilever at its natural frequency. The cantilever is made of silicon nitride with a nominal length of 70 µm, a width of 10 µm, and a thickness of 100 nm. Double clamped cantilevers or more complex geometries such as membrane structures are possible alternatives [15, 16, 17].

The shift in the cantilever's natural frequency also depends on the landing position of the particle. To understand this effect, we need to look at the cantilever's displacement profile or the mode shape of the n^{th} eigenmode $\psi_n(x)$ that can be determined by solving

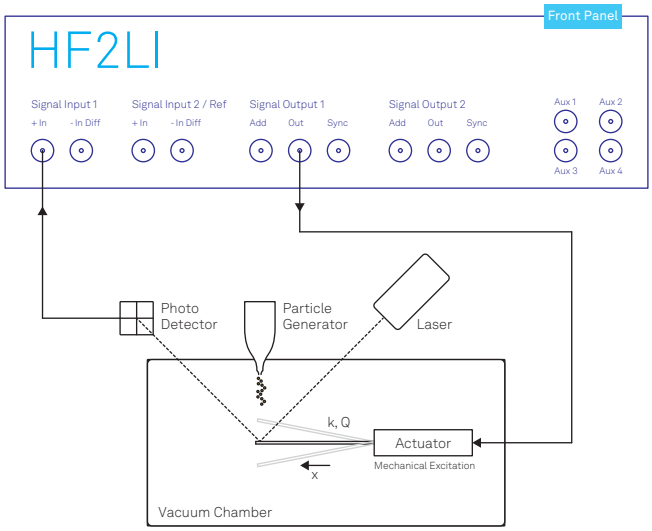

Figure 4. Nanomechanical mass spectrometer that uses an actuated cantilever. The HF2LI Lock-in Amplifier controls this actuation and tracks the cantilever's resonance frequency with its phase-locked loop.

the Euler-Bernoulli equation, yielding

$$\psi_n(x) = \cosh\left(\frac{x\beta_n}{L}\right) - \cos\left(\frac{x\beta_n}{L}\right) + \frac{\cos(\beta_n) + \cosh(\beta_n)}{\sin(\beta_n) + \sinh(\beta_n)} \left(\sin\left(\frac{x\beta_n}{L}\right) - \sinh\left(\frac{x\beta_n}{L}\right)\right), \quad (4)$$

where β_n stands for the n^{th} eigenvalue and L is the cantilever's length. The boundary condition for a single clamped beam is

$$1 + \cosh(\beta_n)\cos(\beta_n) = 0, \quad (5)$$

which yields $\beta_{n=1,2,3,4} = 1.8751, 4.6941, 7.8547, 10.9955$ for the the first four eigenmodes. The frequency shift of the n^{th} eigenmode induced by the added mass is then given by

$$\frac{\Delta f_n}{f_n} = -\frac{1}{2}\frac{\Delta m}{m_r}\psi_n^2(x_0) \quad (6)$$

where Δm is the deposited mass, m_r is the resonator mass, and x_0 is the particle's landing position [18, 19].

A wealth of detection schemes exist to monitor the resonator's motion, including electrical transduction methods such as resistive [14] and capacitive [20] coupling often used in inertial sensors, e.g. MEMS gyroscopes. However, optical transduction methods have demonstrated higher sensitivity and larger measurement bandwidths thanks to the lifted constraint of slow readout circuits [21]. A common optical detection scheme monitors the deflection of a laser beam hitting close to the maximal slope point of a vibrating structure, as illustrated in Figure 4 [22]. The motion of the cantilever changes the position of the deflected

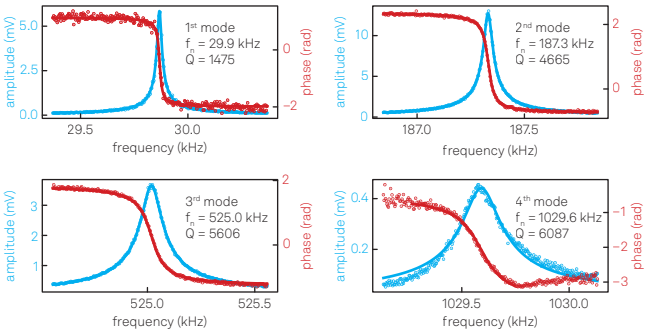

Figure 5. Characterization of the NMS. Resonance peaks and phase delays of the first four flexural vibration modes of the cantilever beam.

light impinging on a quadrant photodetector. This detection scheme transduces the mechanical modulation of the cantilever to a modulated electrical signal. Figure 5 shows the mechanical spectra of the cantilever's first four eigenmodes measured using the LabOne parametric Sweeper.

100-nm-sized gold nanoparticles are deposited on the resonator using an electrospray ionization technique from a solution into a vacuum stage to test the NMS. This technique transfers the particles through a heated capillary at 180 °C to ensure complete solvent evaporation, and then guides them on the cantilever surface using an aerodynamic lens. While particles land on the resonator, the HF2LI Lock-in Amplifier's phase-locked loop (PLL) tracks the frequency shift to capture individual landing events. The closed-loop bandwidth is an important parameter that determines how fast the PLL can track these events. For the most demanding applications, the Zurich Instruments UHFLI Lock-in Amplifier provides up to 300 kHz closed-loop bandwidth [23]. Importantly, the PID Advisor included in the LabOne software simulates the transfer function at each eigenmode using the resonance frequency and quality factor determined by the initial frequency sweep to configure the PLL at the desired bandwidth.

Tracking the frequency shift of two eigenmodes simultaneously is sufficient to extract Δm and x_0 from Equation 6. However, the nodes of a tracked eigenmode are blind to the landing particles. Therefore, tracking more eigenmodes eliminates such blind spots and minimizes errors [24]. The HF2LI equipped with upgrade options HF2LI-MF, HF2LI-PID and HF2LI-PLL can track up to six eigenmodes simultaneously.

NMS can track multiple eigenmodes with 1 part per million (ppm) precision, which is why it can measure the mass of 100-nm-sized gold nanoparticles. Figure 6 (a) shows the relative frequency shifts of the first four eigenmodes induced by individual particle deposition. By applying a mathematical algorithm, it is possible to calculate a mass histogram from the relative

frequency shifts [25]. This results in 10 fg for the mean particle mass as depicted in Figure 6 (b), which is in agreement with expected results [4].

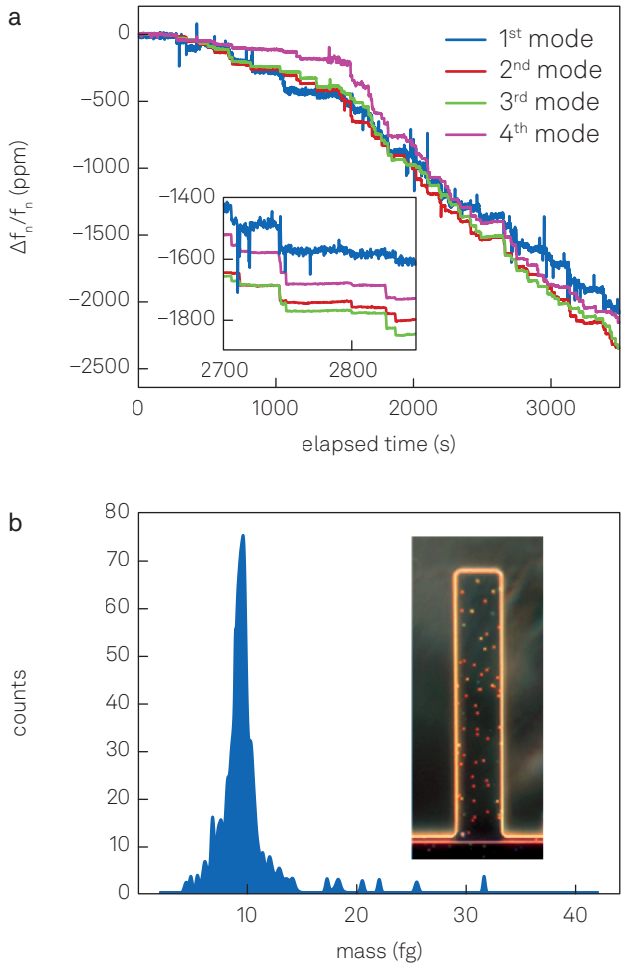

Figure 6. Measurement results with the NMS. (a) Relative frequency shifts of the first four eigenmodes upon 100-nm-sized gold nanoparticle landing events. (inset) Close-up view of the elapsed time between 2700 to 2850 s. (b) Mass distribution of 100-nm-sized gold nanoparticles calculated from the relative frequency shifts measured. (inset) Dark-field optical microscope image of the beam with deposited gold particles visible as orange and red dots.

Transparent microcapillary resonators

Nanomechanical resonators can also work with colloidal samples that require placing the resonator into the suspension liquid. In liquids, however, the viscous drag force decreases the quality factor and the added fluid column increases the effective mass of the resonator, which results in reduced mass resolution. Hence, microcapillary resonators are preferred, especially to classify mass distributions in colloids. They can provide exceptional sensitivity at the 10-attogram level while maintaining a high particle throughput of up to 300 particles per minute [26, 27, 28].

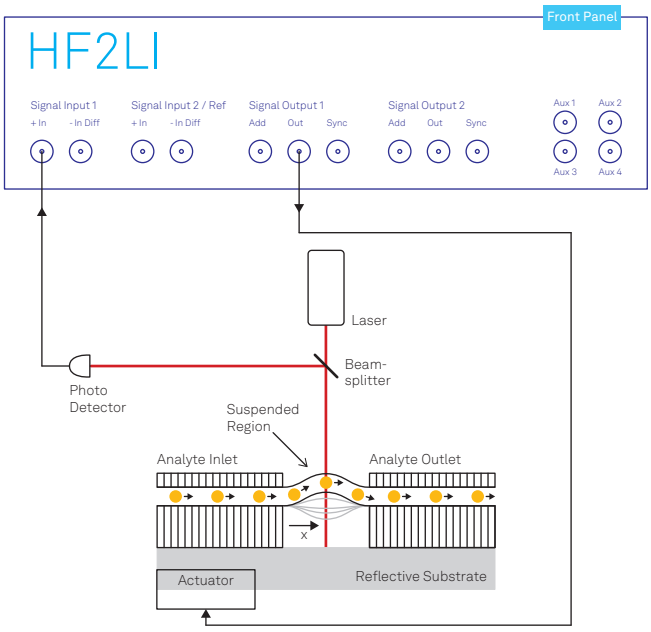

Figure 7. The TMR Scheme. A suspended capillary tube is put into motion by an actuator driven by a Zurich Instruments lock-in amplifier. The back-reflected light impinging on the photodiode carries information on the capillary's motion and on the relative reflectivity of the traversing particles.

To realize this scheme, a microcapillary tube is suspended over a groove of its substrate as illustrated in Figure 7. The same scheme can be realized on a flat substrate by elongating a capillary tube to a double-funnel shape [26]. It can be modeled as a double clamped beam, which has mode shapes given by Equation 4 with the boundary condition

$$1 - \cosh(\beta_n)\cos(\beta_n) = 0. \tag{7}$$

This yields the first four eigenmodes as $\beta_{n=1,2,3,4} = 4.7300, 7.8532, 10.9956, 14.1372$.

Particles traversing the microcapillary tube cause a shift in its resonance frequency that depends on both the particle's buoyant mass and the shape of the eigenmode $\psi_n(x)$. For instance, the maximum frequency shift for the first eigenmode occurs when the particle is approximately at the center of the suspended tube. Figure 8 (a) shows such a shift as a time trace. In higher-order eigenmodes, the frequency shift appears as multiple maxima (data not shown) [5]. While the natural frequencies are in the kHz range, the frequency shifts do not exceed a few Hz. Such small variations do not change the quality factor Q of an eigenmode, and so the frequency shift becomes proportional to the shift in phase delay:

$$\Delta f = \frac{f_r}{2Q}\Delta\varphi. \tag{8}$$

As a result, it is sufficient to capture the phase delay at the initial resonance frequency. This means that

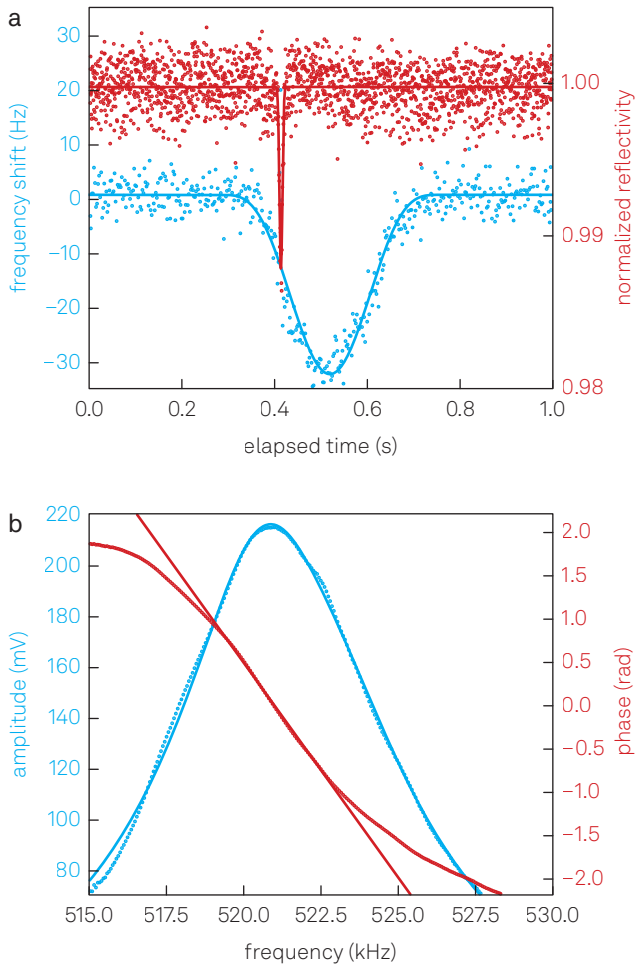

Figure 8. Characterization of the TMR. (a) Frequency shift and normalized reflectivity measured for a passing particle. (b) Mechanical spectrum for the TMR used in this work. Dots correspond to experimental data points and lines are fit results.

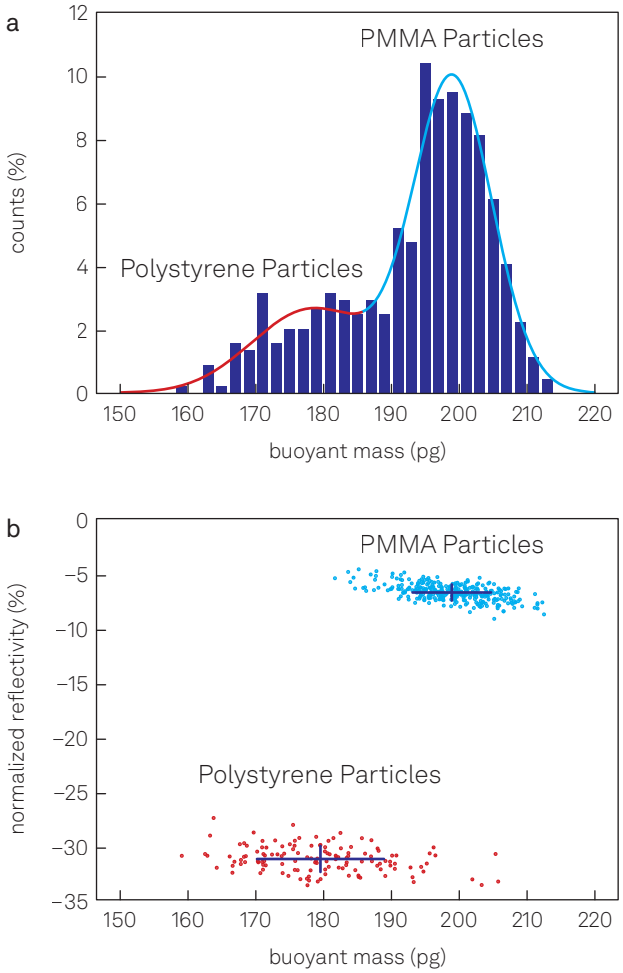

Figure 9. Measurement results with the TMR. (a) Buoyant mass distribution measured (bars) for a mixture of 12.4 µm PMMA and 19 µm PS microparticles and its fit to a double normal distribution (solid line). (b) Scatter plot of buoyant mass and normalized reflectivity in percentage (circles) measured for every single particle. Horizontal and vertical lines indicate the average and the deviation of each particle type. The plots in (b) are adapted from [26] with permission from ACS. Further permissions related to the material excerpted should be directed to the ACS.

the microcapillary resonators can operate in an open-loop configuration and benefit from the entire measurement bandwidth of the lock-in amplifier for measurements with faster particle flow. The two required parameters in Equation 8, Q and f_r, are characterized using the LabOne parametric Sweeper that conveniently provides the resonance frequency, linewidth, and quality factor by fitting a Lorentzian function to the mechanical spectrum shown in Figure 8 (b).

Special care is needed when working with microcapillary resonators because these devices are sensitive to buoyant mass instead of particle mass. For instance, two particles of different materials with different densities and sizes could have the same buoyant mass. Transparent microcapillary resonators (TMRs) solve this problem by providing an additional optical measurement that monitors the intensity of the light reflected from the suspended region as illustrated in Figure 7 [29, 30]. Traversing particles scatter the light and reduce the intensity of the reflected light in different proportions depending on the particle's optical properties. An example of this effect is given in Figure 8 (a), which shows the intensity drop in normalized reflectivity R. This detection scheme transduces both the mechanical modulation of the resonator and the total light intensity of the reflected light to a proportional voltage signal with AC and DC components, respectively. The HF2LI can capture both components simultaneously thanks to its measurement range going from DC to 50 MHz.

Martín-Pérez and collaborators tested the TMR approach with a mixture of monodisperse spherical colloids of poly-methylmetacrylate (PMMA) with 12.4 µm diameter and polystyrene (PS) with 19 µm diameter [5, 6, 26, 31]. Each particle pass is recorded, and the mechanical signal is fitted to the mode shape to obtain the maximum frequency shift. This leads

to the buoyant mass of each particle. The resulting buoyant mass distribution reveals two peaks that correspond to the two particle populations, as illustrated in Figure 9 (a).

Fitting this distribution to a double normal distribution yields two populations with buoyant masses equal to 178±9 pg and 199±6 pg. This measurement agrees with the nominal values of the monodisperse colloids. Although the particles are different in size and density (1.26 g/mL for PMMA and 1.05 g/mL for PS), they produce overlapping buoyant mass distributions. However, when mass data are combined with reflectivity data, we obtain two well-resolved distributions that belong to each particle type as shown in Figure 9 (b). This multiparametric approach makes TMRs a robust particle classifiers against overlapping buoyant masses of different particle types.

Summary

Optomechanical mass sensors provide a non-destructive and direct pathway to probe the mass of particles in various forms. This application note looks at different case studies for aerosol particles, deposited particles in vacuum, and colloids. A common first step in each case is to characterize the system dynamics, which often requires sweeping the frequency and capturing the response of the optomechanical system. The built-in temporal and spectral measurement tools in the LabOne software help characterize the resonator and find the resonance frequency efficiently. The signal generator of Zurich Instruments' lock-in amplifiers drives the resonator. At the same time, its demodulator extracts the desired signal with an adjustable bandwidth for optimizing the signal-to-noise ratio of the measurement. The PLL and PID options of the instrument can then track multiple eigenmodes of the resonator to capture rapid frequency shifts.

Acknowledgments

Zurich Instruments would like to thank Oliver Reich and Ruth Signorell at ETH Zurich, and Oscar Malvar, Daniel Ramos, Adrián Sanz-Jiménez, and Alberto Martín-Pérez in the Bionanomechanics Lab at the Institute of Micro and Nanotechnology of the National Scientific Research Council in Spain (IMN-CSIC) for their cooperation and for sharing experimental results. For further information please contact Zurich Instruments directly on info@zhinst.com or +41 44 515 04 10. We are curious to discuss your experimental requirements.

References

[1] Thomas E Angel, Uma K Aryal, Shawna M Hengel, Erin S Baker, Ryan T Kelly, Errol W Robinson, and Richard D Smith. Mass spectrometry-based proteomics: existing capabilities and future directions. Chem. Soc. Rev., 41(10):3912–3928, May 2012.

[2] Ruedi Aebersold and Matthias Mann. Mass spectrometry-based proteomics. Nature, 422(6928):198–207, March 2003.

[3] Oliver Reich, Grégory David, Kıvanç Esat, and Ruth Signorell. Weighing picogram aerosol droplets with an optical balance. Communications Physics, 3(1):1–8, December 2020.

[4] O Malvar, J J Ruz, P M Kosaka, C M Domínguez, E Gil-Santos, M Calleja, and J Tamayo. Mass and stiffness spectrometry of nanoparticles and whole intact bacteria by multimode nanomechanical resonators. Nat. Commun., 7:13452, November 2016.

[5] Alberto Martín-Pérez, Daniel Ramos, Javier Tamayo, and Montserrat Calleja. Coherent Optical Transduction of Suspended Microcapillary Resonators for Multi-Parameter Sensing Applications. Sensors, 19(23), November 2019.

[6] Alberto Martín-Pérez, Daniel Ramos, Marina L Yubero, Sergio García-López, Priscila M Kosaka, Javier Tamayo, and Montserrat Calleja. Hydrodynamic assisted multiparametric particle spectrometry. Sci. Rep., 11(1):3535, February 2021.

[7] Daniel M. Murphy. Atmospheric science. Something in the air. Science, 307(5717):1888–1890, March 2005.

[8] William C Hinds. Aerosol technology: properties, behavior, and measurement of airborne particles. Wiley, New York, second ed. edition, 1999.

[9] Grégory David, Kıvanç Esat, Irina Ritsch, and Ruth Signorell. Ultraviolet broadband light scattering for optically-trapped submicron-sized aerosol particles. Phys. Chem. Chem. Phys., 18(7):5477–5485, February 2016.

[10] Kıvanç Esat. Characterization of Optically Trapped Aerosol Particles: From Phase Transitions to Photochemical Reactions. PhD thesis, ETH Zurich, 2019.

[11] Lewis Greenspan. Humidity fixed points of binary saturated aqueous solutions. J. Res. Natl. Bur. Stand. A Phys. Chem., 81A(1):89, January 1977.

[12] J L Arlett, E B Myers, and M L Roukes. Comparative advantages of mechanical biosensors. Nat. Nanotechnol., 6(4):203–215, April 2011.

[13] H W Ch Postma, H W Ch. Postma, I Kozinsky, A Husain, and M L Roukes. Dynamic range of

nanotube- and nanowire-based electromechanical systems. Appl. Phys. Lett., 86(22):223105, 2005.

[14] Y T Yang, C Callegari, X L Feng, K L Ekinci, and M L Roukes. Zeptogram-scale nanomechanical mass sensing. Nano Lett., 6(4):583–586, April 2006.

[15] Daniel Ramos, Ian W Frank, Parag B Deotare, Irfan Bulu, and Marko Lončar. Non-linear mixing in coupled photonic crystal nanobeam cavities due to cross-coupling opto-mechanical mechanisms. Appl. Phys. Lett., 105(18):181121, November 2014.

[16] Daniel Ramos, Oscar Malvar, Zachary J Davis, Javier Tamayo, and Montserrat Calleja. Nanomechanical Plasmon Spectroscopy of Single Gold Nanoparticles. Nano Lett., 18(11):7165–7170, November 2018.

[17] Mert Yuksel, Ezgi Orhan, Cenk Yanik, Atakan B Ari, Alper Demir, and M Selim Hanay. Nonlinear Nanomechanical Mass Spectrometry at the Single-Nanoparticle Level. Nano Lett., 19(6):3583–3589, June 2019.

[18] D Ramos, J Tamayo, J Mertens, M Calleja, and A Zaballos. Origin of the response of nanomechanical resonators to bacteria adsorption. J. Appl. Phys., 100(10):106105, November 2006.

[19] Javier Tamayo, Daniel Ramos, Johan Mertens, and Montserrat Calleja. Effect of the adsorbate stiffness on the resonance response of microcantilever sensors. Appl. Phys. Lett., 89(22):224104, November 2006.

[20] Marc Sansa, Marta Fernández-Regúlez, Álvaro San Paulo, and Francesc Pérez-Murano. Electrical transduction in nanomechanical resonators based on doubly clamped bottom-up silicon nanowires. Appl. Phys. Lett., 101(24):243115, December 2012.

[21] Daniel Ramos, Eduardo Gil-Santos, Oscar Malvar, Jose M Llorens, Valerio Pini, Alvaro San Paulo, Montserrat Calleja, and Javier Tamayo. Silicon nanowires: where mechanics and optics meet at the nanoscale. Sci. Rep., 3(1):1–7, December 2013.

[22] D Ramos, J Tamayo, J Mertens, and M Calleja. Photothermal excitation of microcantilevers in liquids. J. Appl. Phys., 99(12):124904, 2006.

[23] Tomás Manzaneque, Peter G Steeneken, Farbod Alijani, and Murali K Ghatkesar. Method to Determine the Closed-Loop Precision of Resonant Sensors From Open-Loop Measurements. IEEE Sens. J., 20(23):14262–14272, December 2020.

[24] S Dohn, W Svendsen, A Boisen, and O Hansen. Mass and position determination of attached particles on cantilever based mass sensors. Rev. Sci. Instrum., 78(10):103303, October 2007.

[25] Jose Jaime Ruz, Oscar Malvar, Eduardo Gil-Santos, Daniel Ramos, Montserrat Calleja, and Javier Tamayo. A Review on Theory and Modelling of Nanomechanical Sensors for Biological Applications. Processes, 9(1):164, January 2021.

[26] Alberto Martín-Pérez, Daniel Ramos, Eduardo Gil-Santos, Sergio García-López, Marina L Yubero, Priscila M Kosaka, Álvaro San Paulo, Javier Tamayo, and Montserrat Calleja. Mechano-Optical Analysis of Single Cells with Transparent Microcapillary Resonators. ACS Sens, 4(12):3325–3332, December 2019.

[27] Jungchul Lee, Wenjiang Shen, Kris Payer, Thomas P Burg, and Scott R Manalis. Toward attogram mass measurements in solution with suspended nanochannel resonators. Nano Lett., 10(7):2537–2542, July 2010.

[28] Max A Stockslager, Selim Olcum, Scott M Knudsen, Robert J Kimmerling, Nathan Cermak, Kristofor R Payer, Vincent Agache, and Scott R Manalis. Rapid and high-precision sizing of single particles using parallel suspended microchannel resonator arrays and deconvolution. Rev. Sci. Instrum., 90(8):085004, August 2019.

[29] Oscar Malvar, Daniel Ramos, Carmen Martínez, Priscila Kosaka, Javier Tamayo, and Montserrat Calleja. Highly sensitive measurement of liquid density in air using suspended microcapillary resonators. Sensors, 15(4):7650–7657, March 2015.

[30] Donghyuk Lee, Joonhui Kim, Nam-Joon Cho, Taewook Kang, Sangken Kauh, and Jungchul Lee. Pulled microcapillary tube resonators with electrical readout for mass sensing applications. Sci. Rep., 6:33799, October 2016.

[31] Alberto Martín-Pérez, Daniel Ramos, Javier Tamayo, and Montserrat Calleja. Nanomechanical Molecular Mass Sensing Using Suspended Microchannel Resonators. Sensors, 21(10), May 2021.